



Mitigation of Tearing Mode Instabilities by Radial AC Magnetic Fields in the STOR-M Tokamak

Sayf Elgamoudi Elgriw^{*1} , Chijin Xiao² 

¹ Department of Nuclear Engineering, Faculty of Engineering, University of Tripoli, Tripoli, Libya

² Department of Physics and Engineering Physics, University of Saskatchewan, Saskatoon, Canada

*Corresponding author email: sayf.gamudi@gmail.com

Received: 02-09-2025 | Accepted: 13-12-2025 | Available online: 15-12-2025 | DOI:10.26629/uzjest.2025.22

ABSTRACT

Generating external radial magnetic fields and studying their effects on tokamak plasmas has been an ongoing topic in fusion research. Experimental studies have shown that externally applied radial magnetic fields can suppress plasma instabilities in tokamaks, particularly tearing mode instabilities. External radial magnetic fields have been successfully implemented in the STOR-M tokamak using ($m = 2, n = 1$) helical coils. However, this system can only produce static magnetic fields. The objective of this work is to design a new coil system capable of producing radial AC magnetic fields for improved tearing mode mitigation in STOR-M. The new system generates phase-varying rotating modes that can be tuned to match the natural frequency of tearing instabilities, which lies in the range of 10-30 kHz. The system consists of 8 toroidally distributed coil sets, each comprising trapezoidal and rectangular coils installed at different poloidal locations around STOR-M. Analytical modeling and numerical simulations have been conducted to determine the coil inductance, radial magnetic field distribution, and the resulting poloidal and toroidal mode spectra. Magnetic fields were calculated using the Biot-Savart law, and Fourier-based modal analysis was applied to identify dominant and sideband modes. A driving circuit consisting of an underdamped series RLC configuration and an H-bridge switching circuit was also analyzed to assess its capability to deliver stable high-frequency AC currents. The results show that the new coil system can generate radial magnetic fields with a dominant (2, 1) mode, accompanied by other sideband modes such as (1, 1) and (2, 7).

Keywords: Tokamak, STOR-M, Tearing Mode Instabilities, Radial Magnetic Fields, Coil Induction, Driving Circuit

تلافي حالات عدم الاستقرار لنمط التمزيق بالحقول المغناطيسية الشعاعية

المتناوبة في توكاماك STOR-M

سيف القمودي^{*1}، تشيجين شياو²

¹ قسم الهندسة النووية، كلية الهندسة، جامعة طرابلس، طرابلس، ليبيا

² قسم الفيزياء والهندسة الفيزيائية، جامعة ساسكاتشوان، ساسكاتون، كندا

ملخص البحث

يُعد توليد المجالات المغناطيسية الشعاعية الخارجية ودراسة تأثيراتها على بلازما التوكاماك موضوعًا مستمرًا في أبحاث الاندماج النووي. وقد أظهرت الدراسات التجريبية أن المجالات المغناطيسية الشعاعية الخارجية قادرة على كبح عدم استقرار البلازما في التوكاماك، ولا سيما عدم استقرار نمط التمزق. وقد تم تطبيق المجالات المغناطيسية الشعاعية الخارجية بنجاح في توكاماك STOR-M باستخدام ملفات حلزونية ($m = 2, n = 1$). مع ذلك، لا يُمكن لهذا النظام سوى إنتاج مجالات مغناطيسية ثابتة. يهدف هذا العمل إلى تصميم نظام ملفات جديد قادر على إنتاج مجالات مغناطيسية متناوبة شعاعية لتحسين تخفيف نمط التمزق في STOR-M. يستطيع النظام الجديد توليد أنماط دوران متغيرة الطور يُمكن ضبطها لتتوافق مع التردد الطبيعي لعدم استقرار التمزق، والذي يقع في نطاق 10-30 كيلوهرتز. يتكون النظام من 8 مجموعات ملفات موزعة حلقيًا، تتألف كل منها من ملفات شبه منحرفة ومستطيلة مثبتة في مواقع قطبية مختلفة حول STOR-M. أُجريت عمليات نمذجة تحليلية ومحاكاة عددية لتحديد محاثة الملف، وتوزيع المجال المغناطيسي القطري، وأطياف الأنماط البوليديّة والطورية الناتجة. حُسبت المجالات المغناطيسية باستخدام قانون بيو-سافار، وطُبّق تحليل الأنماط القائم على تحويل فورييه لتحديد الأنماط السائدة والأنماط الجانبية. كما حُللت دائرة قيادة تتكون من تكوين RLC متسلسل مُخمد جزئيًا ودائرة تبديل H-bridge لتقييم قدرتها على توفير تيارات مترددة عالية التردد مستقرة. تُظهر النتائج أن نظام الملف الجديد قادر على توليد مجالات مغناطيسية قطرية بنمط سائد (2, 1)، مصحوبًا بأنماط جانبية أخرى مثل (1, 1) و (2, 7).

الكلمات الدالة: توكاماك، STOR-M، عدم استقرار نمط التمزق، الحقول المغناطيسية الشعاعية، الحث الملفي، دائرة القيادة

1. Introduction

The use of external radial magnetic fields has been proven to be an essential technique in tokamak fusion research [1]. It has been utilized in many practical applications including, but not limited to, plasma instability control [2], error field correction [3], and plasma rotation modification [4]. The externally applied radial magnetic field can be either a DC or an AC magnetic field, which can be generated by an external coil system. One of the main applications of these external fields is the mitigation and control of tearing mode instabilities. This can be achieved by controlling the frequency and the amplitude of the tearing modes. It has been found that driving current in external coil windings suppresses tearing modes with the same helicity, up to a certain current threshold. Exceeding this threshold may lead to mode locking and, subsequently, plasma disruptions [5].

The Saskatchewan Torus-Modified (STOR-M) tokamak is a small tokamak located at the University of Saskatchewan and is the only device in Canada devoted to magnetic fusion research [6]. STOR-M is currently capable of externally generating static (DC) magnetic fields via an ($m = 2, n = 1$) helical coil winding, where m is the poloidal number and n the toroidal mode number. The coil windings are externally installed on the vacuum chamber of STOR-M at a radius of 17 cm. This coil system has been successfully used to mitigate tearing mode instabilities [7], which is characterized by a reduction in frequency and amplitude of tearing modes. The coil system has also been used to control the toroidal plasma flow [8] as well as edge plasma parameters [9].

The helical coil system currently mounted on the STOR-M Tokamak only works to stabilize the plasma by producing stationary spatial modes which correspond to the dominant tearing mode instabilities. An improvement on this design would be the ability to produce rotating modes, as the instabilities rotate within the plasma at a frequency between 10 kHz and 30 kHz. To do so, an arrangement of externally mounted coils could be used, similar to that installed in J-TEXT tokamak [10]. Each coil can be powered

by an AC current to induce phase differences between the different coil sets, thereby creating rotating modes.

This paper is organized as follows. Section 2 is an overview of the new coil system. Section 3 covers the induction calculations for the coils, followed by the results of the radial magnetic field calculations in Section 4. Section 5 discusses the modal analysis and the mode spectrum generated by the new coil system. The driving circuit analysis and its simulation for the coil system are presented in Section 6. Finally, a short summary and conclusions are given in Section 7.

2. Design Overview

The purpose of this work is to develop a new coil system that will counteract the tearing modes instabilities in the STOR-M Tokamak. As mentioned earlier, the STOR-M Tokamak is already equipped with a helical coil system capable of suppressing the (2, 1) tearing mode. However, this coil system creates only a static radial magnetic field that does not rotate with the instabilities. As a result, the interaction between the coil and the instabilities varies depending on the location of the instabilities. Rotating modes can be generated using a set of external coils, as demonstrated in the J-TEXT Tokamak [10]. Their design consisted of 4 sets of coils equally spaced in the toroidal direction, where each set comprising 3 coils. Sinusoidal currents with variable phase shift between coils were used to generate rotating modes. This design produced a dominant (2, 1) mode, with significant contribution from the (2, 3) and (2, 5) sideband modes. Using the J-TEXT design as a starting point, the possibility of producing more isolated modes will be explored by increasing the number of coils. As shown in Figure 1, the STOR-M tokamak can accommodate up to 16 sets of 3 coils, with each coil's geometry constrained by the physical structure of the tokamak.

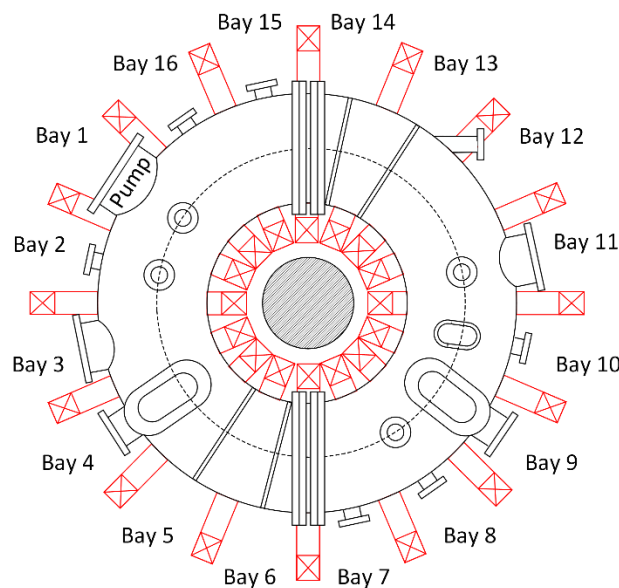


Figure 1. Top view of the STOR-M Tokamak

The new coil system currently being developed for STOR-M consists of sets of coils connected to a power supply and a driving circuit. The coil arrangement consists of 8 sets of external coils installed toroidally at every even-numbered bay (i.e., Bay 2, Bay 4, Bay 6...etc.). Each coil set comprises 3 coils placed poloidally on top, bottom and front sides of the vacuum chamber, all at a radius of 17 cm from the plasma center. The coils mounted on the top and the bottom are trapezoidal in shape, whereas the front coil is rectangular. This coil configuration is expected to be sufficient for targeting the (2, 1) tearing mode, which is the dominant mode instability in STOR-M.

The new coil system will be connected to the DC power supply of the existing helical coil system, which consists of a 50 mF, 450 V fast capacitor bank for fast current ramp-up and a 480 mF, 200 V slow bank for maintaining the current flat-top. An H-bridge circuit will be used to convert the DC output into an AC current. The AC current is generated by switching the voltage across the coils between V and $-V$ at the natural frequency of the circuit. Driving this AC current through the coil system generates an external radial AC magnetic field with controllable phase and frequency. The coil system is designed to operate in the 10-30 kHz range, corresponding to the typical rotation frequency of tearing modes in STOR-M.

3. Coil Induction

The inductance of each trapezoidal coil is a critical parameter in the design of the coil system. This section therefore focuses on calculating the inductance of a trapezoidal coil with arbitrary geometric parameters a , b , γ , and r_w , as shown in Figure 2. Here, a and b are the lengths of two adjacent sides of the trapezoidal coils, γ is the acute base angle, and r_w is the thickness of the coil. For simplicity only the self-inductance of each trapezoidal coil is considered.

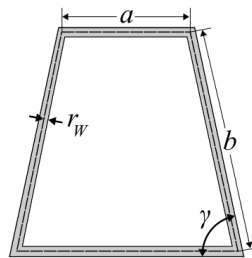


Figure 2. Geometrical parameters for trapezoidal coil

The total self-inductance is made up of an external part, L_{external} , and an internal part, L_{internal} [11]:

$$L = L_{\text{external}} + L_{\text{internal}} \quad (1)$$

The external inductance is given by:

$$L_{\text{external}} = \frac{1}{I} \int_A \mathbf{B}(\mathbf{x}) \cdot d\mathbf{A} \quad (2)$$

where A is the inner area of the coil (the non-shaded interior in Figure 2), I is the current, and $\mathbf{B}(\mathbf{x})$ is the magnetic field generated by the coil. Since the magnetic field is directly proportional to the current, the resulting cancellation leaves the external inductance independent of the input current, making it solely dependent on the coil geometry. The internal inductance term arises from the finite thickness of the coil wire. When a DC current is applied, the current distribution within the wire is approximately homogeneous, leading to an internal inductance of [12]:

$$L_{\text{internal}} = \frac{\mu_r \mu_0}{8\pi} l_w \quad (3)$$

where μ_0 is the permeability of free space, μ_r is the relative magnetic permeability of the wire and l_w is its length. When an AC current is applied, however, the skin effect leads to a current distribution that favors the outer surface of the wire. In this case, the internal inductance is expressed as [13]:

$$L_{\text{internal}} = \frac{l_w}{4\pi r_w} \sqrt{\frac{\mu_r \mu_0}{\pi \sigma f}} \quad (4)$$

where σ is the wire's conductivity and f is the AC frequency. The accuracy of the Equations (3) and (4) depends on the skin depth, which is given by:

$$\delta = \frac{1}{\sqrt{\pi f \mu_r \mu_0 \sigma}} \quad (5)$$

When $r_w/\delta < 1.9$ the error in using Equation (3) is less than or equal to 10%, and when $r_w/\delta > 2.2$ the error in using Equation (4) is less than or equal to 10% [13].

The inductance calculations were performed numerically for both trapezoidal and rectangular copper coils, with the material choice based on the J-TEXT implementation [10]. The relevant input parameters for both the trapezoidal and rectangular coils are listed in Table 1. The AC frequencies required for the design fall in the range of 10 - 30 kHz, corresponding to the typical mode frequency range in STOR-M.

Table 1. Input parameters for inductance calculations

Parameter	Trapezoidal Coil	Rectangular Coil
a	0.13 m	0.20 m
b	0.20 m	0.36 m
γ	80°	90°
μ_r	0.999994	
σ	5.96×10^7 S/m (at 20°C)	

Figure 3 shows the variation with wire thickness, r_w , of the inductance for DC, 10 kHz, 20 kHz, and 30 kHz for the trapezoidal and rectangular copper coils. It should be noted that the ratio r_w/δ is in the range of 1.53 to 15.3, 2.17 to 21.7, and 2.66 to 26.6 for the frequencies of 10 kHz, 20 kHz, and 30 kHz, respectively. Apart from the copper wire with a radius less than 2 mm and frequency of 10 kHz, all these ratios are larger than or equal to 2.2. Therefore, the plots have an associated error of at most 10%.

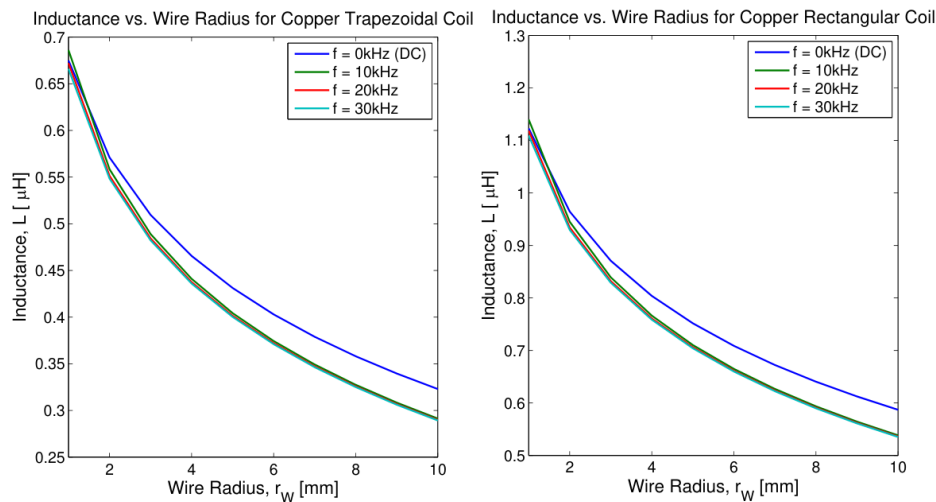


Figure 3. Variation of inductance with wire thickness for trapezoidal and rectangular coils

It is also clear from Figure 3 that the inductance is in the range of 0.3 - 0.7 μH for a trapezoidal coil, and 0.5 - 1.15 μH for the rectangular coil. These values offer an estimated value for the inductance of coils in the design of the coil system. For the purposes of this design, an induction value of 1 μH will be used. When a specific wire radius and operating frequency are chosen, the corresponding values from Figure 3 can be used.

4. Radial Magnetic Field

Calculating the radial magnetic field generated by an arrangement of trapezoidal and rectangular coils is necessary to determine the amount of current required for counteracting the tearing mode instabilities. The primary tool for performing these calculations is the Biot-Savart Law for a line current which is given by [14]:

$$\mathbf{B}(\mathbf{r}) = \frac{\mu_0}{4\pi} \int_C \frac{I d\mathbf{l} \times \mathbf{r}'}{|\mathbf{r}'|^2} \quad (6)$$

where I is the current, C is the curve describing the wire, and $d\mathbf{l}$ is the tangent vector to the curve C at \mathbf{r}' . Equation (6) utilizes the thin wire approximation which assumes that the current is concentrated at the center of the wire. Since the radial magnetic field is calculated far away from the wire (i.e., a distance much greater than r_w from the wire), this approximation is sufficient.

The calculation proceeds by first determining the magnetic field due to a single trapezoidal or rectangular coil in the coil coordinates (x', y', z') , as illustrated in Figure 4(a). This is accomplished by using Equation (6) with C being the piecewise linear curve describing the coil wire. After the field of a single coil is calculated, it is rotated and translated into the torus coordinates (x, y, z) , shown in Figure 4(b).

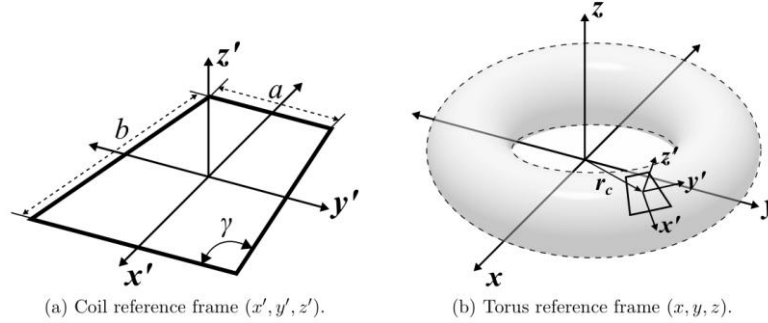


Figure 4. Reference frames for the magnetic field calculation

With the unit vectors for the torus and coil reference frames denoted by $\{\hat{x}, \hat{y}, \hat{z}\}$ and $\{\hat{x}', \hat{y}', \hat{z}'\}$, respectively, the relevant rotation matrix (\mathbf{M}_c) that rotates and translates elements from the coil frame to the torus frame, along with its inverse, is expressed as:

$$\mathbf{M}_c = \begin{pmatrix} \hat{x} \cdot \hat{x}' & \hat{x} \cdot \hat{y}' & \hat{x} \cdot \hat{z}' \\ \hat{y} \cdot \hat{x}' & \hat{y} \cdot \hat{y}' & \hat{y} \cdot \hat{z}' \\ \hat{z} \cdot \hat{x}' & \hat{z} \cdot \hat{y}' & \hat{z} \cdot \hat{z}' \end{pmatrix} \quad \mathbf{M}_c^{-1} = \begin{pmatrix} \hat{x}' \cdot \hat{x} & \hat{x}' \cdot \hat{y} & \hat{x}' \cdot \hat{z} \\ \hat{y}' \cdot \hat{x} & \hat{y}' \cdot \hat{y} & \hat{y}' \cdot \hat{z} \\ \hat{z}' \cdot \hat{x} & \hat{z}' \cdot \hat{y} & \hat{z}' \cdot \hat{z} \end{pmatrix} \quad (7)$$

Denoting \mathbf{B}_c as the magnetic field evaluated in the coil reference frame and assuming the coil is centred at \mathbf{r}_c , as shown in Figure 4(b), the magnetic field in the torus coordinates at a point \mathbf{r} can be calculated by:

$$\mathbf{B}(\mathbf{r}) = \mathbf{M}_c \mathbf{B}_c (\mathbf{M}_c^{-1} (\mathbf{r} - \mathbf{r}_c)) \quad (8)$$

Using Equations (6), (7), and (8), the radial magnetic field contribution from each individual coil can be calculated and added up to obtain the total magnetic field.

Numerical calculations of the magnetic field were carried out for an arrangement of $n = 8$ sets of 3 coils. The top and bottom coils were modelled as trapezoidal, while the front coils were assumed to be rectangular. The geometric parameters of these coils are listed in Table 1. All coils were positioned at $r_T = r_F = r_B = 17$ cm with a major radius of $R = 46$ cm, corresponding to the expected mounting locations on the STOR-M tokamak. A current of ± 1 kA was assigned to the coils in an alternating pattern. Figure 5 shows both a 3D model and a contour plot of the resulting radial magnetic field at $r = 7$ cm, which is the radial location where dominant tearing mode instabilities typically occur [8]. From this figure, it is evident that currents in the order of 1 kA generate a radial magnetic field of approximately 30 G/kA. If the intensity of tearing mode instabilities is assumed to be around 5 G, a current of magnitude

$$I = \frac{5 \text{ G}}{30 \text{ G/kA}} = 167 \text{ A}$$

is required to counteract the instabilities. Therefore, when designing the circuit, a current in the range of $10^2 - 10^3$ A must be taken into account.

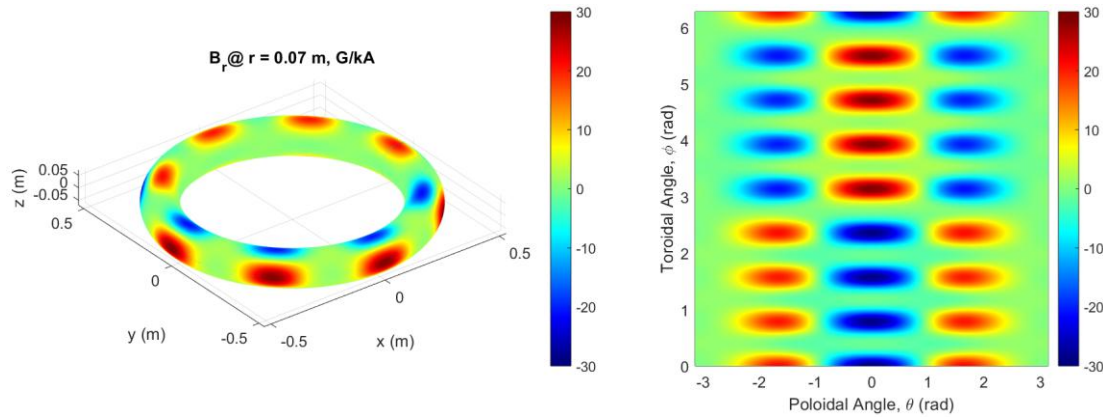


Figure 5. 3D model and contour plot of radial magnetic field generated by the coil arrangement at $r = 7$ cm

5. Mode Spectrum

To determine the full mode spectrum generated by the coil system, the radial magnetic field can be expressed in the same form as that of the tearing mode instabilities. Hence, the radial magnetic field produced by the coil arrays can be written as [15]:

$$B_r(\theta, \phi, t) = \sum_{n,m} B_{r0mn} \cos(m\theta - n\phi + \omega t) \quad (9)$$

where B_{r0mn} is the amplitude of the m and n modes. For simplicity, the above equation can be expressed separately for the toroidal and poloidal components of the magnetic field. The radial magnetic field of the toroidal modes at a fixed poloidal angle θ_0 and time t_0 can be expressed by:

$$B_r(\theta_0, \phi, t_0) = \sum_n (B_{r0n,c} \cos(n\phi) + B_{r0n,s} \sin(n\phi)) \quad (10)$$

where $B_{r0n,c}$ and $B_{r0n,s}$ are the cosine and sine amplitude of the n^{th} toroidal mode. Likewise, the radial magnetic field of the poloidal modes at a fixed toroidal angle ϕ_0 and time t_0 can be written as:

$$B_r(\theta, \phi_0, t_0) = \sum_m (B_{r0m,c} \cos(m\theta) + B_{r0m,s} \sin(m\theta)) \quad (11)$$

The amplitude of the toroidal mode n is therefore:

$$c_n = \sqrt{B_{r0n,c}^2 + B_{r0n,s}^2} \quad (12)$$

To calculate the toroidal mode amplitude c_n , the coefficients $B_{r0n,c}$ and $B_{r0n,s}$ can be evaluated from Equation (10). These coefficients are simply the Fourier series coefficients and can be calculated as follows:

$$B_{r0n,c} = \frac{1}{\pi} \int_0^{2\pi} B_r(\theta_0, \phi, t_0) \cos(n\phi) d\phi \quad (13)$$

$$B_{r0n,s} = \frac{1}{\pi} \int_0^{2\pi} B_r(\theta_0, \phi, t_0) \sin(n\phi) d\phi \quad (14)$$

Similarly, the amplitude of the poloidal mode m is given by:

$$c_m = \sqrt{B_{r0m,c}^2 + B_{r0m,s}^2} \quad (15)$$

and $B_{r0m,c}$ and $B_{r0m,s}$ can be determined in the same manner as the Fourier series coefficients in Equation (11). A modal analysis was performed for an array of 8 coil sets, each consisting of one rectangular coil

at $\theta = 0$ and two trapezoidal coils at $\theta = \pm\pi/2$. The layout of 3 coil sets is shown in Figure 6, and the coil dimensions are already listed in Table 1.

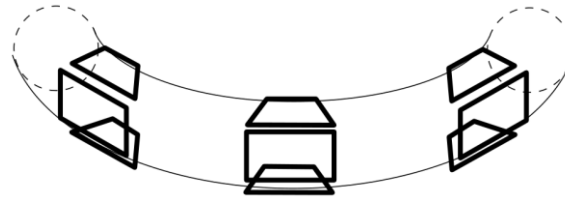


Figure 6. 3 sets of 3-coil arrangement

Using the radial magnetic field formulas developed in Section 4, the resulting magnetic field at fixed poloidal angle (i.e., $\theta = 0$) and $r = 7$ cm is shown in Figure 7(a). The corresponding toroidal modes generated by the coil system is shown in Figure 7(b). It is evident that the mode $n = 1$ is the dominant mode, contributing nearly by 34% of the total mode amplitude. However, there is also significant contribution from other odd-numbered modes like $n = 7$ and $n = 9$.

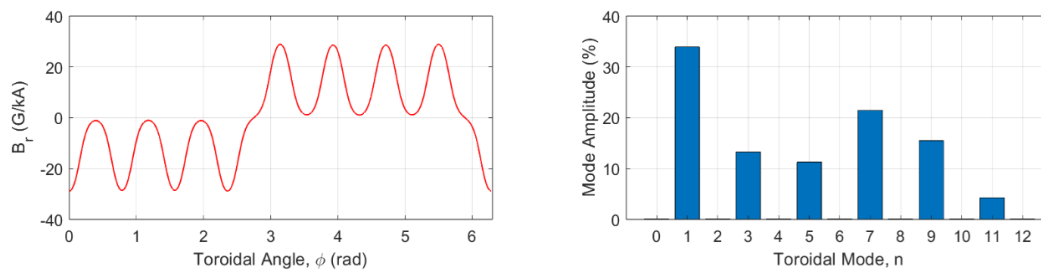


Figure 7. Radial magnetic field and toroidal modes generated by 8 sets of coils at $\theta = 0$ and $r = 7$ cm

The poloidal modes produced by the coil system can also be analysed. Recall that there are only three coils in the poloidal direction, trapezoidal coils at $\theta = \pm\pi/2$ and a rectangular coil at $\theta = 0$. With only three coils there is not much control over the choice of the poloidal mode. However, the resulting poloidal modes can still be examined. Figure 8(a) shows the radial magnetic field calculated at $\phi = 0$ and $r = 7$ cm. The corresponding poloidal mode generated by the coils is shown in Figure 8(b). It is clear that the dominant modes correspond to $m = 1$ and $m = 2$, contributing respectively by 34.3% and 47.7% to the total mode amplitude.

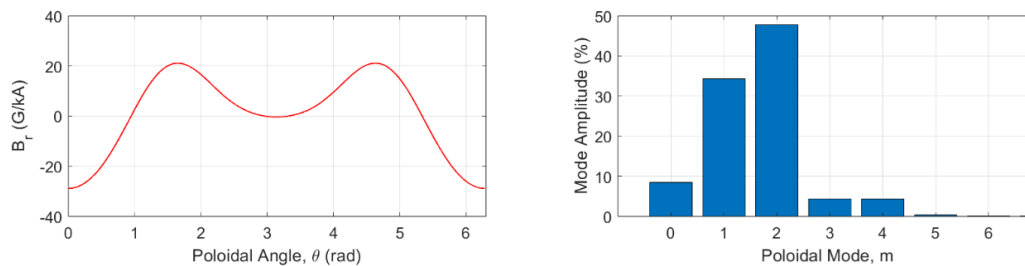


Figure 8. Radial magnetic field and poloidal modes generated by 8 sets of coils at $\phi = 0$ and $r = 7$ cm

The complete mode spectrum produced by the coil system is presented in Figure 9, which shows the normalized amplitudes of the toroidal and poloidal modes calculated using Equations (13) and (14). It is clearly seen that the coil system can generate a strong (2, 1) mode, contributing with approximately 15% of the total spectrum amplitude. Other significant sideband modes, such as (1, 1) and (2, 7) modes, also contribute to the mode spectrum by 12.7% and 10.8%, respectively.

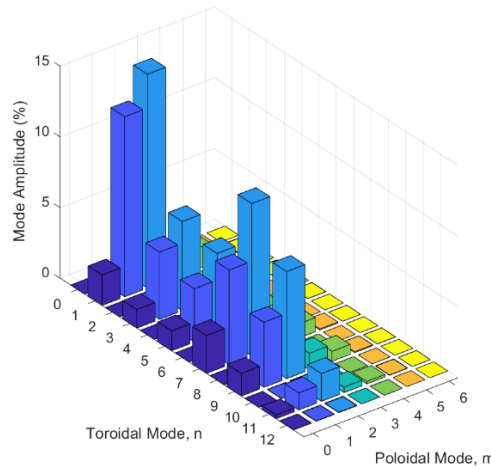


Figure 9. Complete mode spectrum generated by the coil system

6. Driving Circuit

The purpose of the driving circuit is to drive an AC (sinusoidal) current through each coil. An AC current, as opposed to a DC current, is used to control the phase differences between the coils. The phase differences allow the magnetic field profiles generated by the coil system to rotate along with the tearing mode instabilities, thereby more effectively suppressing these instabilities. The frequency range of the modes is in the range of 10 kHz to 30 kHz, which is also the operational frequency range considered for the driving circuit. Each coil is treated as an inductive load, L , in an underdamped series RLC circuit, as shown in Figure 10.

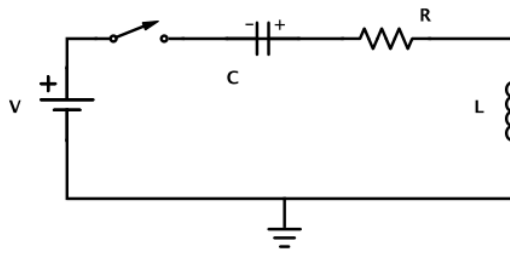


Figure 10. Series RLC Circuit with a voltage source

The capacitor is initially charged to a voltage equal in magnitude but opposite in polarity to that of the DC voltage source V . Once the switch is closed, current begins to flow in the circuit. For the underdamped case, the general expression for the current waveform can be written as [16]:

$$i(t) = I_0 \cos(\omega_d t) e^{-\alpha t} + \frac{V - RI_0 - \frac{q_0}{C}}{\omega_d L} \sin(\omega_d t) e^{-\alpha t} \quad (17)$$

which reduces to the special case when the current starts from zero (i.e., $I_0 = 0$):

$$i(t) = \frac{V - \frac{q_0}{C}}{\omega_d L} \sin(\omega_d t) e^{-\alpha t} \quad (18)$$

where V is the voltage source, q_0 is the initial charge on the capacitor, C is the capacitance, L is the coil inductance, and ω_d is the damped natural frequency of the circuit given by:

$$\omega_d = \sqrt{\omega_0^2 - \alpha^2} = \sqrt{\frac{1}{LC} - \frac{R^2}{4L^2}} \quad (19)$$

where R , L , and C are the resistance, the inductance, and the capacitance of the coil, respectively. The current will gradually decay over time as the capacitor charges. To eliminate this effect, the voltage

polarity must be reversed at the point of current zero-crossing, as illustrated in Figure 11. The capacitor charge may not be zero at the instant when the voltage polarity is reversed, which changes the initial conditions of the circuit. Therefore, the current amplitude will vary after each zero-crossing until it reaches a steady state.

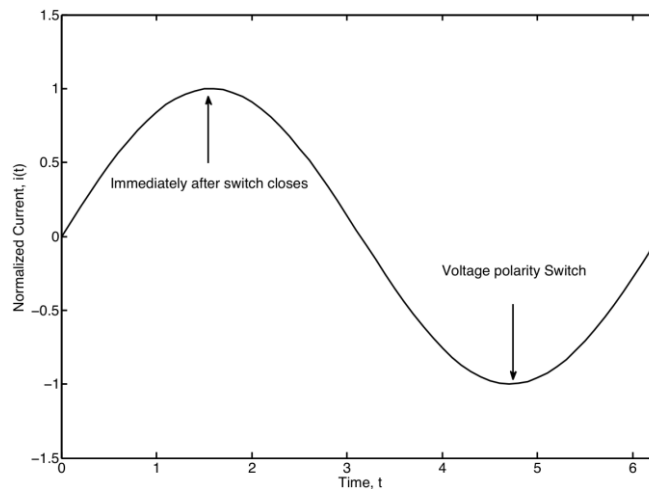


Figure 11. Underdamped series RLC current with voltage polarity switching

A common approach for generating an alternating current from a DC voltage source is through the use of an H-bridge circuit. The general configuration of an H-bridge is shown in Figure 12. In this configuration, switches $S1$ and $S2$ operate at the same frequency, while switches $S3$ and $S4$ also operate together but out of phase with $S1$ and $S2$. This switching pattern causes the voltage across the load to alternate between V and $-V$ at the same frequency as the switches. As a result, the current will alternate through the load. Insulated-Gate Bipolar Transistor (IGBT) power modules are typically used as switches due to their high voltage and current ratings. For an underdamped series RLC circuit, the IGBT switches operate at a driving frequency approximately equal to the damped natural frequency ω_d of the load.

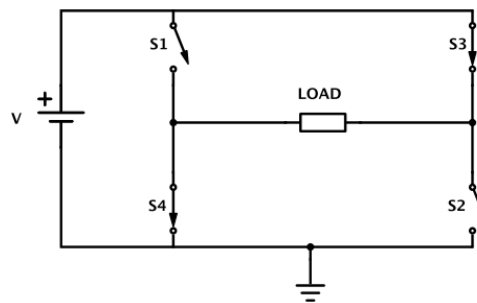


Figure 12. Schematic of H-bridge circuit

A numerical simulation was carried out to determine whether, and at what point, a steady state (i.e., a consistent current amplitude and frequency) is reached in the inductive load. The simulation uses Equation (18) to calculate the current through the load using the following input values: source voltage $V = 100$ V, resistance $R = 0.1$ Ω , inductance $L = 24$ μH , and capacitance $C = 5$ μF , all connected in series. The simulation evaluates the current at each time step t and detects a sign change in the current. When the current crosses zero, the initial conditions I_0 (which should be ≈ 0) and q_0 are updated and the voltage V changes polarity. The resulting current waveform across the load and its corresponding wavelet spectrum are shown in Figure 13. The wavelet spectrum is a useful tool for simultaneously analysing transient signals in the time-frequency domain.

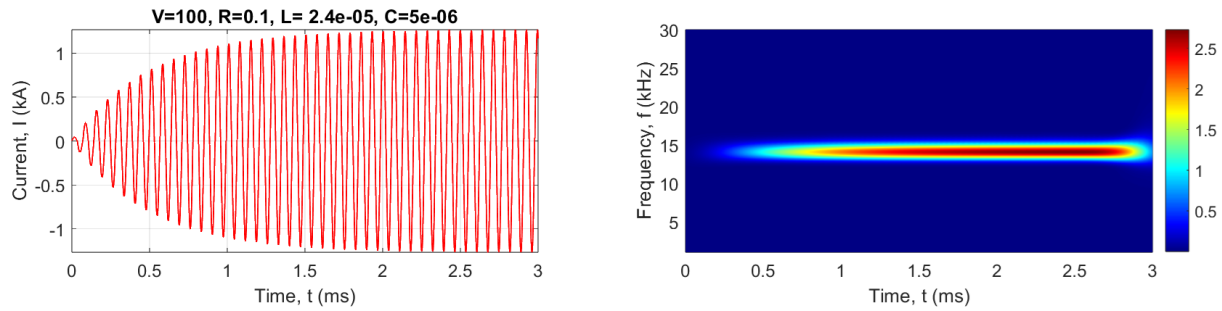


Figure 13. Current waveform driven in the load and the corresponding wavelet spectrum

Based on the input parameters used in the simulation, the damped natural frequency of the series RLC system can be determined as follows:

$$\omega_0 = \frac{1}{\sqrt{LC}} = \frac{1}{\sqrt{24 \mu\text{H} \times 5 \mu\text{F}}} = 91287 \text{ rad/s, and}$$

$$\alpha = \frac{R}{2L} = \frac{0.1 \Omega}{2 \times 24 \mu\text{H}} = 2083 \text{ rad/s}$$

Therefore, the damped natural frequency is:

$$\omega_d = \sqrt{\omega_0^2 - \alpha^2} = \sqrt{(91287 \text{ rad/s})^2 - (2083 \text{ rad/s})^2} = 91263 \text{ rad/s or } 14525 \text{ Hz}$$

It is evident from Figure 13 that the current reaches a steady-state amplitude of around 1.25kA at a frequency of 14.5 kHz, which is approximately equal to ω_d . This indicates that choosing a driving frequency approximately close to ω_d produces a relatively stable sinusoidal current through the inductive load. It is also noted that the current waveform stabilizes after roughly 2 ms, which is negligible compared to a typical plasma discharge duration of 25 ms in STOR-M. The fact that the current stabilizes within a much shorter time than the discharge duration shows that voltage polarity switching for a series RLC circuit is an effective approach for producing an alternating current in the inductive coil system.

7. Summary and Conclusions

The main objective of this work was to develop a conceptual design for a new coil system consisting of 8 sets of 3 trapezoidal and rectangular coils, mounted on the STOR-M Tokamak at different poloidal and toroidal locations. This coil array can produce external radial magnetic fields capable of mitigating the dominant tearing instabilities that arise in the plasma during tokamak operation.

Currently, an ($m=2, n=1$) helical coil system is already installed on the STOR-M Tokamak which has been successfully used to suppress tearing mode instabilities as well as to modify other plasma parameters. A key improvement on this design is the ability to produce modes which rotate at the same frequency as the tearing mode instabilities in the plasma, which is typically in the range of 10-30 kHz.

By driving AC currents with different phases through each of these coils via an H-bridge circuit, a rotating radial magnetic field with variable frequency and phase can, in principle, be generated to suppress the tearing mode instabilities. Analytical models and numerical simulations were conducted to calculate the coil induction, the external radial magnetic field and the mode spectrum generated by the new coil system at $r = 7$ cm, which is the radial location where dominant tearing mode instabilities are most commonly observed in STOR-M.

The preliminary results showed that the coil system can produce a dominant (2, 1) mode, accompanied by other sideband modes such as (1, 1) and (2, 7) modes. The driving circuit was also analysed to

determine the optimal parameters for the coil system as well as to calculate the coil currents required for effective mode suppression.

8. Acknowledgment

This work was sponsored by the Natural Sciences and Engineering Council of Canada (NSERC) and the Sylvia Fedoruk Canadian Center for Nuclear Innovation.

REFERENCES

- [1] T. C. Hender *et al.*, "Effect of resonant magnetic perturbations on COMPASS-C tokamak discharges," *Nucl. Fusion*, vol. 32, no. 12, pp. 2091–2117, 1992.
- [2] L. Frassinetti *et al.*, "Resonant magnetic perturbation effect on tearing mode dynamics," *Nucl. Fusion*, vol. 50, no. 3, pp. 035005-1–035005-13, 2010.
- [3] R. J. Buttery *et al.*, "Error field mode studies on JET, COMPASS-D and DIII-D, and implications for ITER," *Nucl. Fusion*, vol. 39, no. 11Y, pp. 1827–1835, 1999.
- [4] K. H. Finken *et al.*, "Toroidal plasma rotation induced by the dynamic ergodic divertor in the TEXTOR tokamak," *Phys. Rev. Lett.*, vol. 94, no. 1, pp. 015003-1–015003-5, 2005.
- [5] Q. Hu *et al.*, "Effect of externally applied resonant magnetic perturbations on resistive tearing modes," *Nucl. Fusion*, vol. 52, no. 8, pp. 083011-1–083011-11, 2012.
- [6] A. Hirose *et al.*, "STOR-M Tokamak design and instrumentation," *Phys. Canada*, vol. 62, no. 3, pp. 111–120, 2006.
- [7] S. Elgriw *et al.*, "Control of magnetic islands in the STOR-M tokamak using resonant helical fields," *Nucl. Fusion*, vol. 51, no. 11, pp. 113008-1–113008-10, 2011.
- [8] S. Elgriw *et al.*, "Modification of plasma rotation with resonant magnetic perturbations in the STOR-M tokamak," *Plasma Phys. Control. Fusion*, vol. 58, no. 4, pp. 045002-1–045002-11, 2016.
- [9] S. Elgriw *et al.*, "Effect of resonant magnetic perturbations on edge plasma parameters in the STOR-M tokamak," *Radiat. Eff. Defects Solids*, vol. 173, no. 1–2, pp. 31–44, 2018.
- [10] B. Rao *et al.*, "First observation of rotation acceleration of magnetic island by using rotating resonant magnetic perturbation on the J-TEXT tokamak," *Plasma Phys. Control. Fusion*, vol. 55, no. 12, pp. 122001-1–122001-5, 2013.
- [11] F. W. Grover, *Inductance Calculations: Working Formulas and Tables*. Mineola, NY, USA: Dover, 2004.
- [12] C. R. Paul, *Inductance: Loop and Partial*. Hoboken, NJ, USA: Wiley, 2010.
- [13] K. L. Kaiser, *Electromagnetic Compatibility Handbook*. Boca Raton, FL, USA: CRC Press, 2005.
- [14] J. D. Jackson, *Classical Electrodynamics*, 3rd ed. New York, NY, USA: Wiley, 1999.
- [15] A. H. Boozer, "Plasma equilibrium with rational magnetic surfaces," *Phys. Fluids*, vol. 24, no. 11, pp. 1999–2003, Nov. 1981.
- [16] J. W. Nilsson and S. A. Riedel, *Electric Circuits*, 11th ed. Boston, MA, USA: Pearson, 2020.